Cell Chemical Biology, Volume *27*

Supplemental Information

Identification of a Covalent Molecular Inhibitor of Anti-apoptotic BFL-1 by Disulfide Tethering

Edward P. Harvey, Zachary J. Hauseman, Daniel T. Cohen, T. Justin Rettenmaier, Susan Lee, Annissa J. Huhn, Thomas E. Wales, Hyuk-Soo Seo, James Luccarelli, Catherine E. Newman, Rachel M. Guerra, Gregory H. Bird, Sirano Dhe-Paganon, John R. Engen, James A. Wells, and Loren D. Walensky

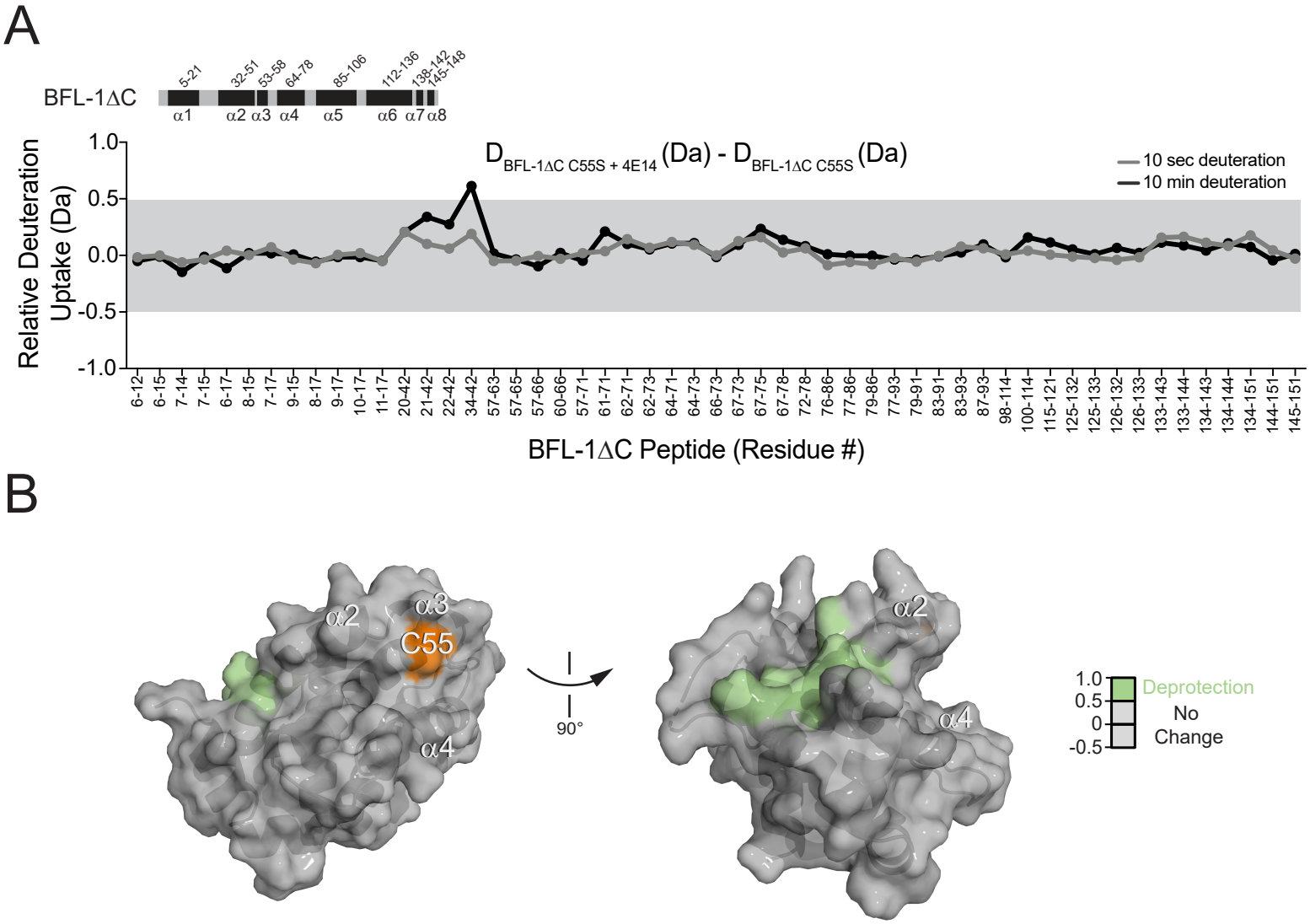
A
BFL-1ΔC
5-21
32-51
53-58
64-78
85-106
112-136
138-142
145-148
α1
α2 α3
α4
α5
α6 α7 α8
D BFL-1ΔC C55S + 4E14 (Da) - D BFL-1ΔC C55S (Da)
10 sec deuteration
10 min deuteration
Relative Deuteration Uptake (Da)
1.0
0.5
0.0
-0.5
-1.0
6-12
6-15
7-14
7-15
6-17
8-15
7-17
9-15
8-17
9-17
10-17
11-17
20-42
21-42
22-42
34-42
57-63
57-65
57-66
60-66
57-71
61-71
62-71
62-73
64-71
64-73
66-73
67-73
67-75
67-78
72-78
76-86
77-86
79-86
77-93
79-91
83-91
83-93
87-93
98-114
100-114
115-121
125-132
125-133
126-132
126-133
133-143
133-144
134-143
134-144
134-151
144-151
145-151
BFL-1ΔC Peptide (Residue #)
B
α2
α3
C55
α4
90°
α2
α4
1.0
0.5
0
-0.5
Deprotection
No Change

Figure S1

Figure S1, Related to Figure 2. Conformational consequences of 4E14 interaction with BFL-1ΔC C55S.

(A) A deuterium difference plot showing the relative deuterium incorporation of BFL-1ΔC C55S conjugated to 4E14 minus that of apo BFL-1ΔC C55S, as measured at the indicated time points. Each identified peptide is indicated in order on the x-axis with the relative protection displayed on the y-axis. The changes outside of the grey shaded region are above the significance threshold of 0.5 Da. Data are representative of two biological replicates. All HXMS data used to create this figure can be found in Data File S1.

(B) The region of relative change in deuterium uptake for BFL-1ΔC C55S/4E14 vs. apo BFL-1ΔC is mapped onto the structure of BFL-1ΔC for the 10 minute time point. The relative level of deprotection is indicated by the color scale.

See also Table S2 and Data File S1.

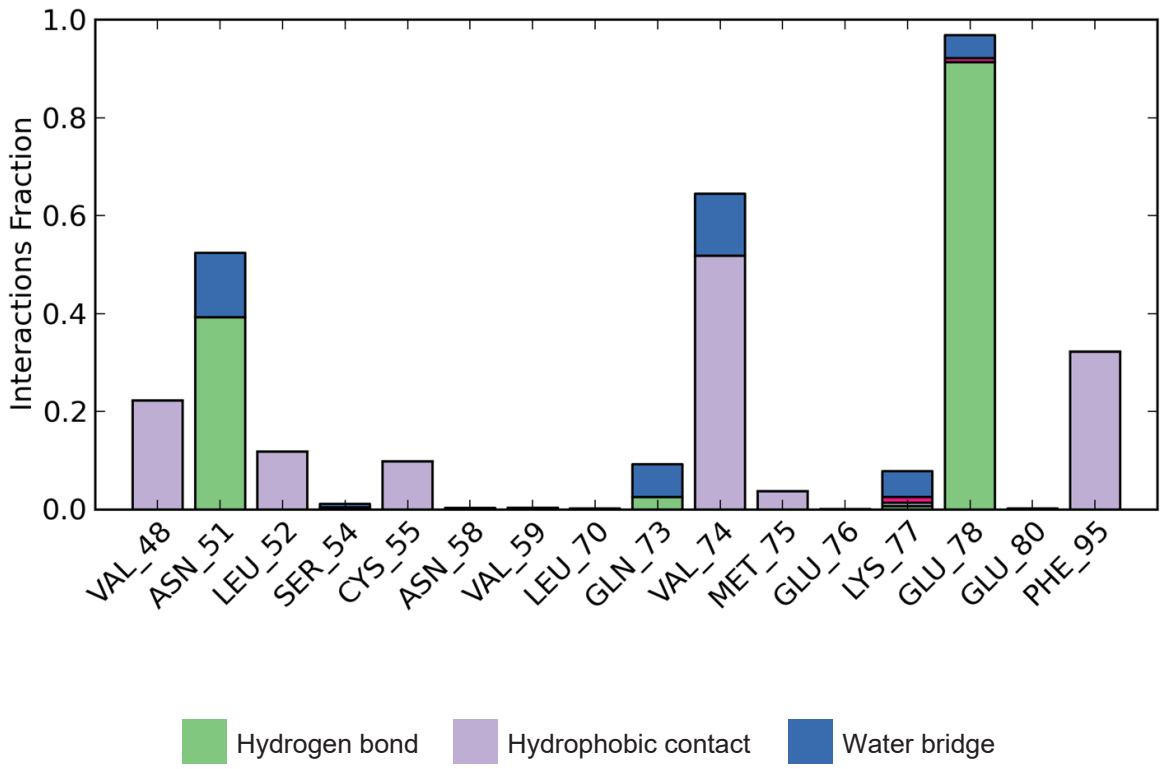
Interactions Fraction
1.0
0.8
0.6
0.4
0.2
0.0
VAL_48
ASN_51
LEU_52
SER_54
CYS_55
ASN_58
VAL_59
LEU_70
GLN_73
VAL_74
MET_75
GLU_76
LYS_77
GLU_78
GLU_80
PHE_95
Hydrogen bond
Hydrophobic contact
Water bridge

Figure S2

Figure S2, Related to Figure 3. Molecular dynamics simulation of the 4E14/BFL-1ΔC interaction.

BFL-1ΔC residues contacted by the 4E14 ligand, as predicted by molecular dynamics simulation of the ligand/protein interaction. Hydrogen bond, green; hydrophobic contacts, purple; water bridges, blue.

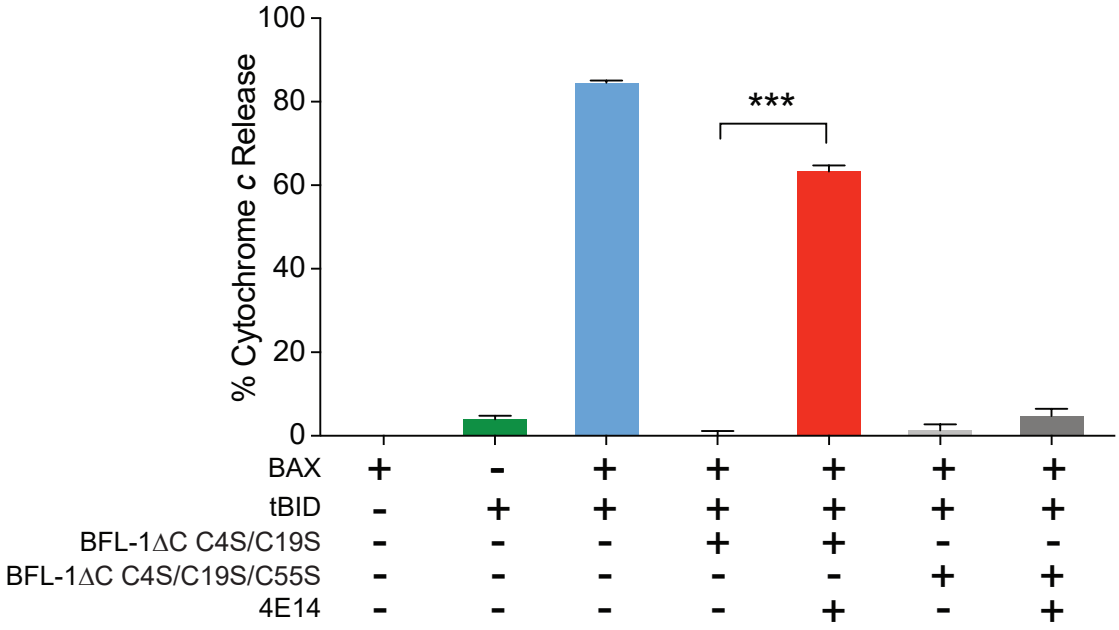
100
80
60
40
20
0
% Cytochrome c Release
***
BAX + - + + + + +
tBID - + + + + + +
BFL-1ΔC C4S/C19S - - - + + - -
BFL-1ΔC C4S/C19S/C55S - - - - - + +
4E14 - - - - + - +

Figure S3

Figure S3, Related to Figure 4. Functional inhibition of BFL-1 by 4E14 in mitochondrial cytochrome *c* release assays is dependent on C55.

Percent cytochrome *c* release from BAX/BAK-deficient mouse liver mitochondria treated with tBID, BAX, and/or BFL-1ΔC C4S/C19S or BFL-1ΔC C4S/C19S/C55S in the presence or absence of 4E14. Data are mean ± S.E.M. for experiments performed in technical triplicate and repeated (two biological replicates) with independent preparations of compound, proteins, and mitochondria. BAX, 100 nM; BFL-1ΔC C4S/C19S and BFL-1ΔC C4S/C19S/C55S, 1 μM; tBID, 40 nM; 4E14 conjugated to BFL-1 proteins at molecule:protein ratio of 5:1. ***, $p<0.0001$ by unpaired Student's t-test.

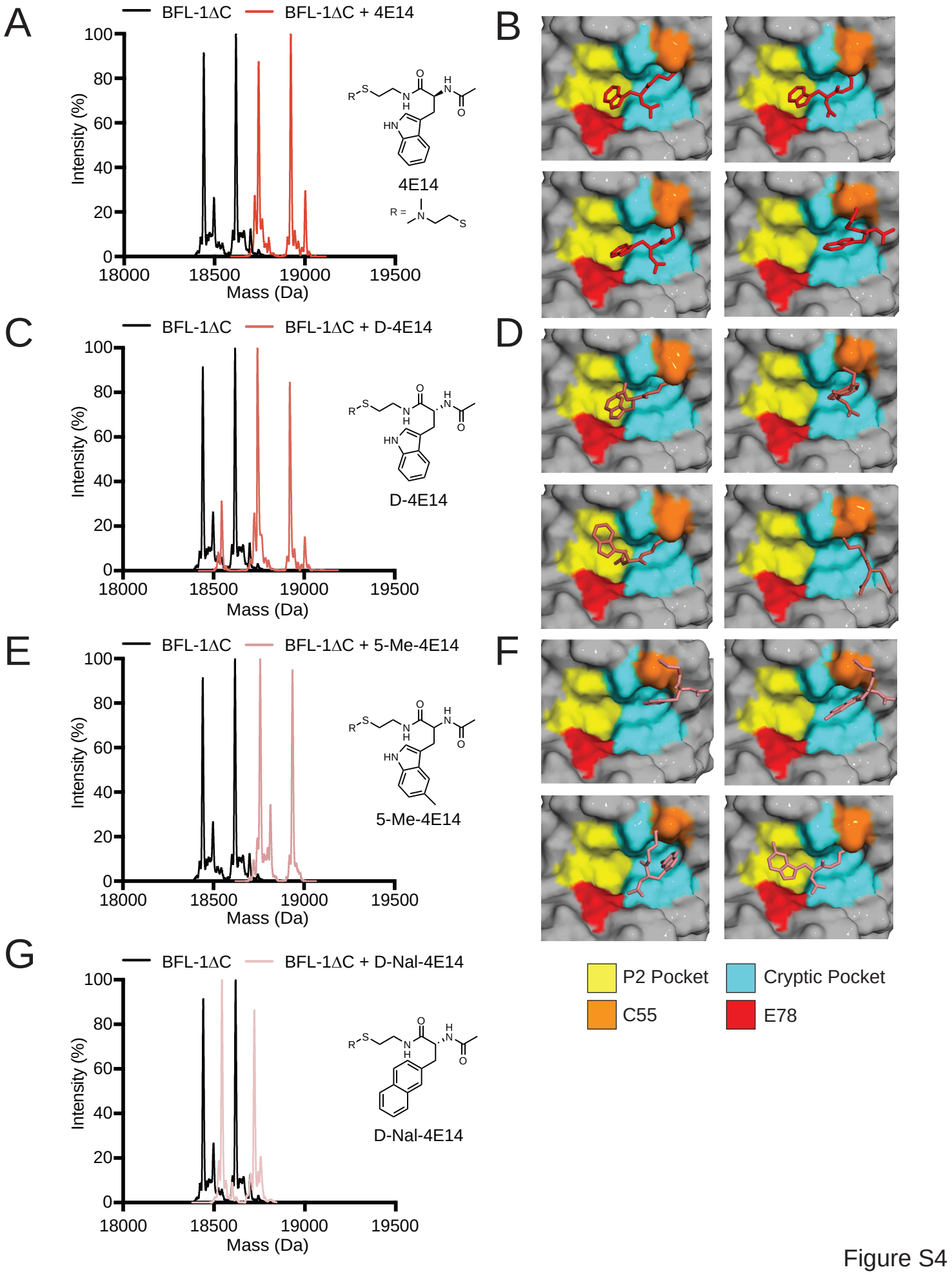
A
BFL-1ΔC
BFL-1ΔC + 4E14
Intensity (%)
Mass (Da)
4E14
B
C
BFL-1ΔC
BFL-1ΔC + D-4E14
D-4E14
D
E
BFL-1ΔC
BFL-1ΔC + 5-Me-4E14
5-Me-4E14
F
G
BFL-1ΔC
BFL-1ΔC + D-Nal-4E14
D-Nal-4E14
P2 Pocket
Cryptic Pocket
C55
E78

Figure S4

Figure S4, Related to Figure 4. Docking analyses of 4E14 analogs at the canonical groove of BFL-1ΔC.

(A) Derivatization of His_6-BFL-1ΔC C4S/C19S by 4E14 (M+304), as measured by intact mass spectrometry (molecule:protein, 5:1; left peak, BFL-1 minus Met plus H_2O; right peak, BFL-1).

(B) Docking analysis of 4E14 positioned the indole moiety at the P2 pocket in three of four poses, in addition to hydrogen bonding between the indole nitrogen and E78. The N-acetyl group was shown to engage the cryptic pocket subjacent to C55 in these poses, while a single pose (bottom right) placed the indole in the cryptic pocket with the acetyl group displaced outward.

(C) Derivatization of His_6-BFL-1ΔC C4S/C19S by the D-enantiomer of 4E14 (M+304), as measured by intact mass spectrometry (molecule:protein, 5:1; left peak, BFL-1 minus Met plus H_2O; right peak, BFL-1).

(D) Docking analysis of D-4E14 positioned the indole at the BFL-1 P2 pocket in only one pose (top left), with the linker and N-acetyl group displaced outward (rather than engaging the cryptic site) in order to accommodate the alternative stereochemistry. Whereas one pose featured the indole and N-acetyl groups bound to the cryptic pocket (top right), two others showed no significant binding interactions of the indole moiety (bottom).

(E) Derivatization of His_6-BFL-1ΔC C4S/C19S by 5-Me-4E14 (M+319), as measured by intact mass spectrometry (molecule:protein, 5:1; left peak, BFL-1 minus Met plus H_2O; right peak, BFL-1).

(F) Docking analysis of 5-Me-4E14 positioned the methyl indole at the cryptic pocket in three distinct orientations, with only one pose featuring additional engagement of the

cryptic pocket by the N-acetyl moiety (bottom left). In one pose (bottom right), the indole was positioned to enable hydrogen bonding between the indole hydrogen and E78 but the added bulk of the methyl group precluded insertion into the P2 pocket (bottom right). (G) Derivatization of His_6-BFL-1ΔC C4S/C19S by N,N-dimethylcysteamine (M+104) rather than D-Nal-4E14, specifically (*R*)-2-acetamido-*N*-(2-mercaptoethyl)-3-(naphthalen-2-yl)propanamide, as measured by intact mass spectrometry (molecule:protein, 5:1; left peak, BFL-1 minus Met plus H_2O; right peak, BFL-1).

4E14 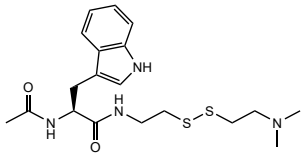

5M16 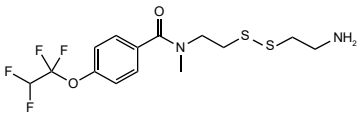

2C11 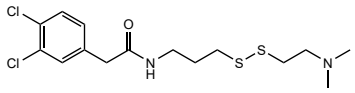

3I03 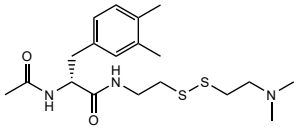

2B22 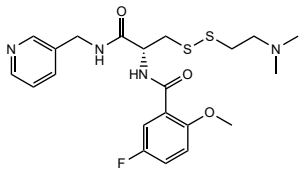

2G15 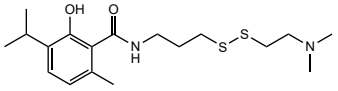

2F20 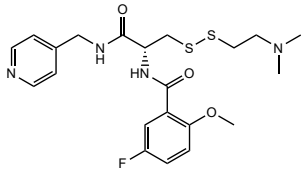

1P09 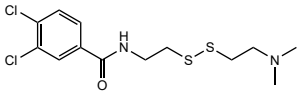

5A12 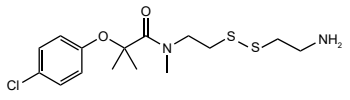

3N11 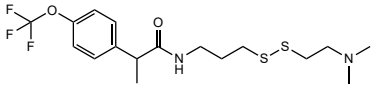

3O12 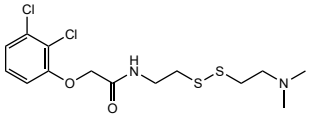

2B12 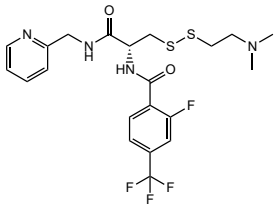

3P13 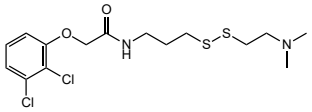

1M05 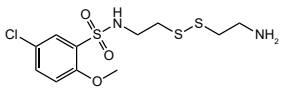

1D09 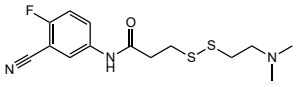

2P09 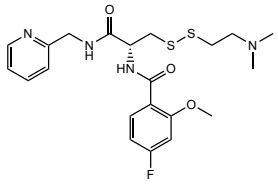

3L15 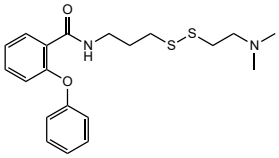

3A20 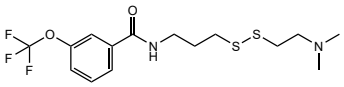

3E06 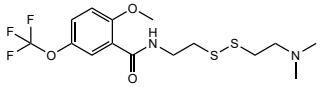

3P05 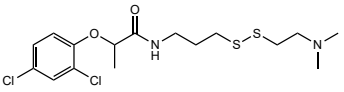

3F15 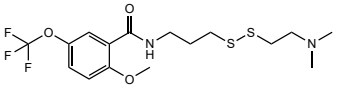

4A18 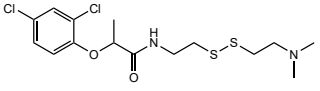

1B08 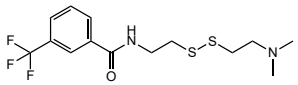

3P13 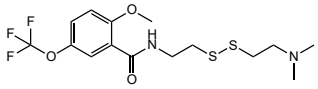

5M06 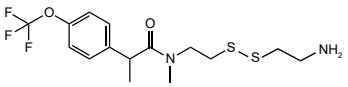

1A19 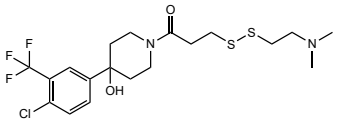

1F15 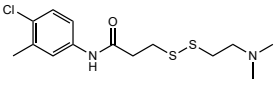

1J12 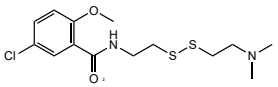

4B13 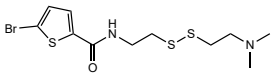

1P03 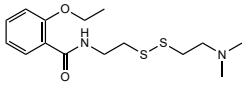

3L07 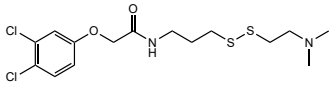

Table S1

Table S1, Related to Figure 1. Chemical structures of small molecule hits from the disulfide tethering screen of BFL-1ΔC C4S/C19S. Small molecule hits are listed in rank order (vertically) of inducing a rightward shift of the FITC-BID BH3/BFL-1 binding isotherm.

Data Set	BFL-1ΔC C4S/C19S	BFL-1ΔC C4S/C19S + 4E14	BFL-1ΔC C55S	BFL-1ΔC C55S + 4E14
HDX reaction details	Final D_2O concentration=94.7%, pH_{read}=7.2, 21 °C. See also footnote a			
HDX time course	10 sec, 10 min			
HDX controls	4 undeuterated		2 undeuterated	
Back-exchange	30-35%			
Number of peptides	56 followed; 61 identified			
Sequence coverage	85.1%			
Average peptide length Redundancy	10.74 a.a.			
Replicates	3 biological		2 biological	
Repeatability	+/- 0.15 relative Da			
Meaningful differences	> 0.5 Da			

[a] 18-fold dilution with labeling buffer [50 mM Tris pD 7.6, 150 mM NaCl, 99.9% D_2O]. 1:1 dilution with quench buffer [4M guanidinium chloride, 200 mM potassium phosphate pH 2.34, 0.72 M TCEP, H_2O]

Table S2

Table S2, Related to Figure 2. Data summary and list of experimental parameters for HXMS analyses of BFL-1ΔC C4S/C19S and its conjugate with 4E14.